Integrated Modeling of Microwave Food Processing and Comparison with Experimental Measurements

R. Akarapu[1], B. Q. Li[1], Y. Huo[1], J. Tang[2] and F. Liu[2]

[1]School of Mechanical and Materials Engineering
[2]Department of Bioengineering Systems
Washington State University, Pullman, WA 99164 – 2920

This paper presents an integrated electromagnetic and thermal model for the microwave processing of food packages. The model is developed by combining the edge finite element formulation of the 3-D vector electromagnetic field in the frequency domain and the node finite element solution of the thermal conduction equation. Both mutual and one-way coupling solution algorithms are discussed. Mutual coupling entails the iterative solution of the electromagnetic field and the thermal field, because the physical properties are temperature-dependent. The one-way coupling is applicable when the properties are temperature independent or this dependence is weak. Mesh sensitivity and shape regularity for the edge element based formulation for computational electromagnetics are discussed in light of available analytical solutions for a simple wave guide. The integrated model has been used to study the electromagnetic and thermal phenomena in a pilot scale microwave applicator with and without the food package immersed in water. The calculated results are compared with the experimentally measured data for the thermal fields generated by the microwave heating occurring in a whey protein gel package, and reasonably good agreement between the two is obtained.

Submission Date: August 2004

Acceptance Date: October 2005

INTRODUCTION

In comparison with conventional thermal processes for food sterilization such as canning and pasteurization, microwave processing has the advantage of providing rapid volumetric heating. This rapid heating results from the direct interaction between electromagnetic fields and foods hermetically sealed in microwave transparent pouches or trays [DeCareau; 1985]. Pilot-scale laboratory trials show that microwave heating significantly reduces the time needed for products to reach the desired temperatures for commercial sterilization. Microwave heating also improves the organoleptic quality, appearance, and nutritional value of many foods. Moreover, the use of microwave processing increases the level of automation, improves productivity, and reduces adverse environmental impacts.

Keywords: modeling, food processing, sterilization

Microwave food processing is a very complicated process that depends on dielectric properties, product size and geometry, design of applicators, and other variables [Metaxas; 1996] [Tang et al.; 1999a & 1999b]. The basic principles of microwave heating and their applications in food processing are described in textbooks [Metaxas & Meredith; 1983] [Metaxas; 1996]. Perkins [1980], an early investigator on the subject, presented a simple model for microwave heating, where he assumed an exponential decay of power absorption from the surface of a heated material towards its interior and studied temperature characteristics of boiling point drying processes. Similar approaches were later used by Zeng and Faghri [1994] and Lu *et al.* [1998] to investigate the microwave thawing and drying of foods. While useful for a crude approximation, the assumption of exponential decay in general is invalid during microwave food processing [Watanabe & Ohkawa; 1978]. In fact, recent studies showed that full 3-D calculations are required for these systems [Neophytou & Metaxas; 1998].

Metaxas and his colleagues have developed a variety of electromagnetic field models using the finite

element method for microwave food processing. The techniques used both frequency domain and time domain formulations. Thermal issues, however, are not considered in their models. Zhang and Datta [2000] recently presented a finite element model for the microwave processing of foods. Their calculations involved the use of two commercial packages, one (EMAS) for computational electromagnetics and the other (NASTRAN) for computational heat transfer. The linkage between the two is achieved through basic UNIX script commands. The numerically predicted temperature distributions were also compared with experimental measurements in a microwave oven. Their results showed that when the physical properties are dependent on temperature, a fully coupled model is required for an accurate representation of interacting electromagnetic and thermal fields. For cases in which the temperature dependence is weak, a de-coupled solution gives a reasonably good representation.

The finite difference time domain (or FDTD) method has also been used for microwave heating modeling [Zhao & Turner; 1996]. The FDTD method uses a three-dimensional central difference approximation for Maxwell's curl equations in space and a central difference scheme for time matching. It is a time-domain method in that the transient calculation is continued either until the fields in the simulation region reach a steady-state situation for a continuous sinusoidal excitation, or until the fields converge to zero for a pulse excitation. This method contrasts the finite element solution of the frequency-based equations. Recently, Haala & Wiesbeck [2000] applied the FDTD method to compute the electromagnetic field and the temperature distributions, taking into consideration the conductive and radiative heat transfer. Their results revealed that for the materials being studied and the conditions being applied, hybrid ovens (those heated by combined microwave and conventional heating) supplied better temperature uniformity in the load than either microwave or conventional ovens alone. The FDTD method is, in general, difficult to apply to the problems with complex geometries that are often encountered in food processing [Peyre et al.; 1997]. This limitation may be alleviated by using unstructured finite volume approaches [Piperno et al.; 2003].

In this paper, we present a computational model, with a full integration of 3-D electromagnetic heating and thermal phenomena, for microwave food sterilization applications. The motivation is derived from the need to develop a better understanding of the electromagnetic and thermal phenomena in industrial scale microwave applicators for food sterilization applications. Moreover, an efficient computational model is needed to help guide the development of the laboratory and pilot-scale microwave systems for commercial food processing that is currently being undertaken at WSU. Experience has shown that an experimentally validated numerical model can play an important role in both developing a fundamental understanding of and providing useful guidelines for process design and optimization. The model development is based on the frequency domain formulation of the full 3-D electromagnetic fields described by the Maxwell equations. To ensure the divergence-free requirement of the magnetic field, the vector finite element formulation, which uses the element-edge based vector shape functions, is employed. The electric heating source is then calculated from the field distributions and fed as an input to a thermal model, which is developed based on the traditional finite element formulation that uses the node-based formulation. Both mutual coupling and one-way coupling between electromagnetic and thermal models are considered in the integral model. The integral model development, mesh-sensivity testing, and a comparison of the model predictions with both analytical solutions and experimental measurements taken on the microwave heating of packaged foods in a pilot-scale microwave applicator are presented.

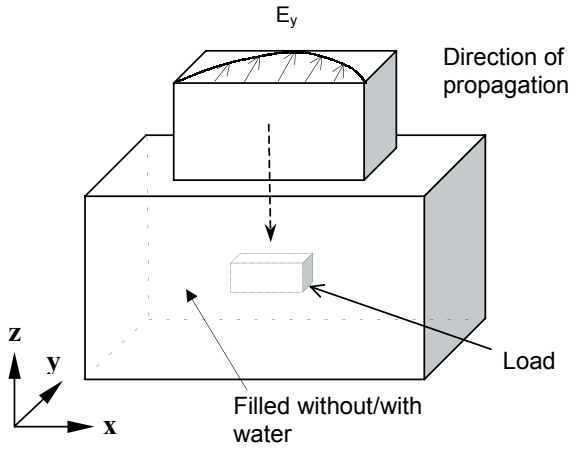

Figure 1. *Schematic representation of microwave applicator system.*

PROBLEM STATEMENT

The microwave applicator system under consideration is a pilot-scale microwave food processing unit and is schematically shown in Figure 1, where two rectangular waveguides are coupled to each other. The top part of the system is the standard WR-975 waveguide with a cross-section of 248mm x 124mm and a height of 522.9 mm; the bottom one is an oversized waveguide with a cross-section of 496mm x 248mm and a height of 100mm. The food package of 140×100×30 (mm^3) is fixed at the center of the bottom part of the applicator.

An electric field of the TE_{10} mode with a frequency 915 MHz is applied at the top to produce the dissipated electrical power that is absorbed by the food load with its initial and environmental temperatures set at the room temperature (300 K).

The development of the electromagnetic-thermal model can be divided into two steps. First, the electric and magnetic fields inside the waveguide are simulated using the finite element method to calculate the dissipated power in the food package. Second, the temperature distribution inside the food piece is computed with the dissipated power as the source term. The differential form of Maxwell's equations is the most widely used representation to solve the boundary-value electromagnetic problems. Maxwell's equations, however, are coupled partial differential equations that have more than one unknown value. Therefore, the vector wave equation derived from the Maxwell's equations combined with the energy equation is taken as the governing equations to simulate the microwave heating problems [Metaxas; 1996],

$$\nabla \times \frac{1}{\mu_r} \nabla \times \mathbf{E}(\mathbf{r}) - k_0^2 \varepsilon_c \mathbf{E}(\mathbf{r}) = -j\omega\mu_0 \mathbf{J}_i \tag{1}$$

where μ_r (= μ/μ_o) is the relative magnetic permeability, ε_c (= $\varepsilon' - j\sigma_e/\omega\varepsilon_0$) results from a combination of the conduction current ($\sigma\mathbf{E}$) and displacement current ($j\omega(\varepsilon' + j\varepsilon'')\mathbf{E}$), with $\sigma_e = \omega\varepsilon'' \varepsilon_0 + \sigma$, J_i the incident current density, and k_0 the system parameter, $k_0^2 = \omega^2\mu_0\varepsilon_0$. The symbols used are the same as those in the standard electromagnetic textbooks [Kraus and Fleisch; 1998]. Specifically, μ_0 stands for the magnetic permeability of free space, ε_0 the permittivity of free space, σ_e the effective conductivity, ω the frequency of the harmonic field and $j=(-1)^{(1/2)}$. Eq. (1) automatically satisfies the divergence free condition, $\nabla \cdot (\varepsilon_0 \varepsilon_c \mathbf{E}) = 0$, when μ_r is considered a constant. Note also that $\mathbf{E}(\mathbf{r})$ is generally a complex field variable and is denoted by $\mathbf{E}$ for the sake of simplifying the notation unless otherwise indicated.

The solution of the above equation is subjected to appropriate boundary conditions governing the electric and magnetic fields. For most microwave thermal processing applications, a metal cavity and/or waveguide is used. Thus, along the wall surface, we have the tangential electric field equal to zero,

$$\mathbf{E}_t = \mathbf{n} \times \mathbf{E} = 0 \tag{2}$$

and at the opening port we have either excitation or transmission, resulting in the following generic boundary condition[Jin; 1993][Volakis et al.; 1998],

$$\mathbf{n} \times (\nabla \times \mathbf{E}) + \gamma \mathbf{n} \times (\mathbf{n} \times \mathbf{E}) = \mathbf{U}^{inc}$$
for the port with wave incident. (3)

$$\mathbf{n} \times (\nabla \times \mathbf{E}) + \gamma \mathbf{n} \times (\mathbf{n} \times \mathbf{E}) = 0$$
for the port with wave being transmitted. (4)

With the electric field $\mathbf{E}$ known, the energy absorbed by dielectric materials such as packaged foods or microwave heating source Q is given by the following expression,

$$Q(\mathbf{r}) = \frac{1}{2}\sigma_e(T)\,\mathbf{E} \cdot \mathbf{E}^* \tag{5}$$

When the dielectric constant is a function of temperature, as often occurs, a mutually coupled solution is required because the dielectric constants must be updated using the temperature field, which in turn is affected by the microwave heating. Microwave heating takes place either in air or in other fluid media, and the heat transfer between the sample and the medium can be modeled using either the radiation boundary condition or Newton's cooling law or both [Akarapu; 2003].

The thermal field in a dielectric material exposed to microwave incidence is governed by the following partial differential equation,

$$\rho C_p \frac{\partial T}{\partial t} = \nabla \cdot (\kappa \nabla T) + Q \tag{6}$$

where ρ is the density of the food package, C_p the specific heat, κ the thermal conductivity. For the system under consideration, the boundary condition is relatively simple and is prescribed by the heat balance through radiation into the environment,

$$-\kappa \hat{\mathbf{n}} \cdot \nabla T = \varepsilon_s \sigma_s \left(T^4 - T_\infty^4\right) \tag{7}$$

where ε_s is the surface emissivity, σ_s the Stefan-Boltzmann constant, and T_∞ the ambient temperature. Here the convective effect is ignored because the thermally-induced free convection inside the microwave cavity is negligible.

The governing equations, Eqs. (1) and (6), reveal that the electromagnetic and thermal fields in the microwave processing systems may be coupled in two ways. One way is mutual coupling. This happens when the electric field property is a function of temperature. Studies show that such coupling can be important in both microwave and thermal field distributions. Because mutual coupling requires a coupled solution of both microwave and thermal fields at each time step during the thermal simulations, this process can be computationally expensive. The other

way is one-way coupling. This happens when the dielectric constant of the food package is either a weak function of temperature or not a function of temperature at all. In the case of one-way coupling, the electromagnetic field needs to be calculated only once, thereby substantially reducing the computational effort.

EDGE FINITE ELEMENT FORMULATION

The finite element formulation starts with the three-dimensional wave equation, or Eq. (1). After multiplying the equation by a vector weighting function (**W**) and integrating over the microwave cavity (or computational domain), one obtains the following integral, which is often referred to as weak form [Jin; 1993],

$$\iiint_V \mathbf{W}\cdot\left(\nabla\times\frac{1}{\mu_r}\nabla\times\mathbf{E}-k^2\quad{}_c\mathbf{E}\right)dV=-\iiint_V j\quad\mu_0\mathbf{W}\cdot\mathbf{J}_i dV \tag{8}$$

Making use of the vector Green's theorem identity,

$$\iiint_V\left[\frac{1}{\mu_r}(\nabla\times\mathbf{W})\cdot(\nabla\times\mathbf{E})-\mathbf{W}\cdot(\nabla\times\frac{1}{\mu_r}\nabla\times\mathbf{E})\right]\frac{1}{\mu_r}dV = \iint\frac{1}{\mu_r}(\mathbf{W}\times\nabla\times\mathbf{E})\cdot\mathbf{n}dS \tag{9}$$

the second order differential terms can be integrated by parts,

$$\iiint_V\left(\frac{1}{\mu_r}\nabla\times\mathbf{E}\cdot\nabla\times\mathbf{W}-k^2\varepsilon_c\mathbf{W}\cdot\mathbf{E}\right)dV = \iint_S\left[\frac{1}{\mu_r}(\mathbf{W}\times\nabla\times\mathbf{E})\cdot\mathbf{n}\right]dS-\iiint_V j\omega\mu_o\mathbf{W}\cdot\mathbf{J}_i dV \tag{10}$$

where $\mathbf{J}_i$ is the incident current density. Because the surface integral exists only on the surface, the boundary condition described by Eqs. (3)-(4) can be used to transform the above equation to,

$$\iiint_V\left(\frac{1}{\mu_r}\nabla\times\mathbf{E}\cdot\nabla\times\mathbf{W}-k^2\varepsilon_c\mathbf{W}\cdot\mathbf{E}\right)dV = -\iint_S\left[\gamma_e(\mathbf{n}\times\mathbf{E})\cdot(\mathbf{n}\times\mathbf{W})+\mathbf{W}\cdot\mathbf{U}^{inc}\right]dS - \iiint_V j\omega\mu\,\mathbf{W}\cdot\mathbf{J}_i dV \tag{11}$$

To ensure that the calculated electric field is divergence free, a numerical treatment is needed. One of the common procedures is to use the penalty method, as has been done in incompressible fluid flow calculations [Huo and Li; 2004]. A better choice, however, is to use the vector edge-based element shape functions. This approach is taken in the present study. For this purpose, tetrahedral elements are used to discritize the computational domain V. Over each tetrahedron, the vector electric field is defined along the edges, and the vector edge shape functions $\mathbf{N}_k(\mathbf{r})$ are constructed as follows,

$$\mathbf{N}_{7-k}(\mathbf{r})=\frac{b_k}{6V_e}(\mathbf{r}_{(7-k)1}\times\mathbf{r}_{(7-k)2})+\frac{b_k b_{(7-k)}}{6V_e}\mathbf{e}_{(7-k)}\times\mathbf{r} \tag{12}$$

where k=1,2…6, V_e= volume of tetrahedron, $\mathbf{e}_k$ = unit vector of the k[th] edge and b_k= length of the k[th] edge of the tetrahedron.

With the vector edge shape function so chosen, the electric field **E** within a tetrahedron can be expanded using the shape function as,

$$\mathbf{E}=\sum_{i=1}^{6}E_i\mathbf{N}_i \tag{13}$$

where E_i is the electric field along the ith edge of the element. Substituting this function into Eq. (11) and carrying out the necessary numerical integration over an element, one has the following matrix equation for the discretized electric fields defined along the element edges,

$$[K^e]\{\mathbf{E}^e\}+[B^e]\{\mathbf{U}^{inc^e}\}=\{\mathbf{F}^e\} \tag{14}$$

where the matrices are calculated using the following expressions,

$$K^1_{ij}=\iiint_{V_e}\left(\frac{1}{\mu_r}\nabla\times\mathbf{N}_i\cdot\nabla\times\mathbf{N}_j-k^2\varepsilon_c\mathbf{N}_i\cdot\mathbf{N}_j\right)dV$$

$$B^e_{ij}=\iint_{S_e}\mathbf{S}_i\cdot\mathbf{S}_j\,dS$$

$$C_{ij}=\iint_{S_e}\gamma_e(\mathbf{n}\times\mathbf{N}_i)\cdot(\mathbf{n}\times\mathbf{N}_j)dS=\iint_S\gamma_e(\mathbf{S}_i)\cdot(\mathbf{S}_j)dS$$

$$F^e_i=-\iiint_{V_e}j\omega\mu_0\mathbf{N}_i\cdot\mathbf{J}_i dV$$

$$K^e_{ij}=K^1_{ij}+C_{ij}$$

Assembling the elemental equations we have the final global matrix equation as follows,

$$[\mathbf{K}]\{\mathbf{E}\} + [\mathbf{B}]\{\mathbf{U}^{inc}\} = \{\mathbf{F}\} \quad (15)$$

which can be solved for the unknown vector fields defined by **E**.

The finite element formulation for heat transfer problems is well known and has been reported in our early publications [Huo and Li; 2004]. The energy equation is solved by using the Galerkin finite element method. The standard finite element procedure leads to the following matrix equation for the nodal temperature distribution,

$$N_T \frac{dT}{dt} + L_T \cdot T = G_T \quad (16)$$

where the matrix coefficients are calculated by,

$$N_T = \iiint_v \rho C_p \theta\theta^T dV$$
$$L_T = \iiint_v \kappa \nabla\theta \cdot \nabla\theta^T dV$$
$$G_T = \iiint_v Q\theta dV$$

with θ being the finite element shape functions. For these calculations, node-based elements are used. To couple the thermal and electromagnetic calculations, the electromagnetic fields are first solved with an assumed temperature distribution. The heating source is then calculated using Eq. (5) and fed into the thermal calculations for an updated temperature field. The calculated temperature is then used to obtain an updated electromagnetic field distribution and then the new temperature field. The procedure is repeated until convergence is achieved. This coupling procedure can be applied to both steady state and transient calculations. In cases where the dielectric constant is nearly independent of temperature, the electromagnetic field calculations need to be calculated only once. Both the mutual and one-way coupling algorithms have been incorporated in the present model.

COMPUTATIONAL ASPECTS

It is well known that the edge finite element formulation for the 3-D electromagnetic fields results in a huge sparse matrix. Efficient numerical methods are needed for solving the sparse systems of linear algebraic equations. A large number of research articles and books have been published on this subject [George and Liu; 1984]. The methods for solving the matrix may be classified into the iterative and direct categories. Although iterative methods have the advantage of reducing computer storage needs, they are difficult to converge to an accurate order and in general are slower than the direct methods, which require more memory but no iteration. A rule of thumb is that whenever memory is affordable a direct method should be used. Of course, blind use of the direct method without a careful account for sparseness will lead to a disaster for finite element computations.

There are four distinct phases (ordering, storage allocation, factorization, and triangular solution) in the direct method to solve for a sparse matrix arising from finite element formulations [George and Liu; 1984]. Ordering is key, and, unfortunately, is theoretically proven to be heuristic. A direct sparse matrix solver employs the LU decomposition but only exploits the non-zero elements in the triangular factor **L** of a matrix **A** if **A** is a structurally symmetric matrix. The direct method takes advantage of the data structure from the ordering phase and performs symbolic factorization, sparse symmetric factorization, and back-substitution. The present study implements the algorithms discussed in [George and Liu; 1984]. The available ordering algorithms are compared in order to reduce either computer storage or computer execution time or a combination of the two. The band scheme and the skyline scheme are relatively easily to implement but are not necessarily efficient. Three ordering schemes in this category, Quote Minimum Degree, Multiple Minimum Degree, and Nested Dissection, are studied. The other ordering methods, Quotient Tree and One-Way Methods, are also applied and their performances are compared with the above three. All these schemes have been incorporated in our code, and extensive testing has been made. The comparative numerical study suggests that the Multiple Minimum Degree ordering algorithm is the most efficient method for solving the electromagnetic problems under consideration. With an optimal reordering, the matrix is then symbolically factorized and finally solved by the general sparse matrix solver, which takes the full advantage of the data structure generated by the ordering phase. Often, the factorization and back-substitution phases are the most time consuming and thus are implemented in a parallel computing environment. Many of these algorithms are available in literature [Demmel et al.; 1999(a)][Demmel et al.; 1999(b)].

EXPERIMENTAL PROCEDURE

In order to verify the simulation results, some experiments were performed with an applicator cavity made of aluminum plates with dimensions as mentioned in section 2. The microwave power was generated by a commercial 5 kW 915 MHz microwave power source manufactured by Microdry Company (Microdry Model IV-5 Industrial Microwave generator, Microdry Incorporated, Crestwood, KY). The microwave power

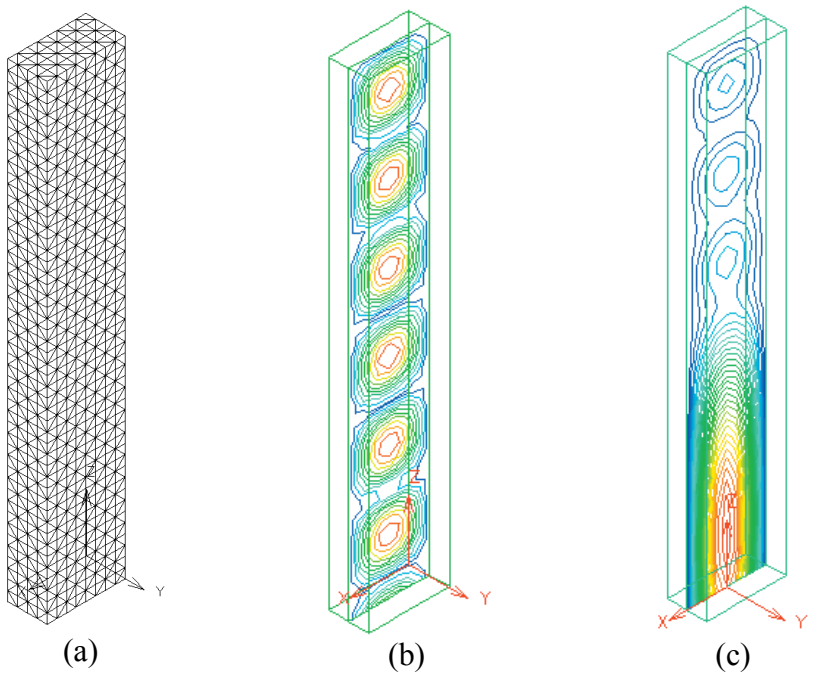

Figure 2. *Mesh plot and contour plots of the electric field modulus for the shorted waveguide (a) mesh plot; (b) lossless waveguide ($\varepsilon_c = 2.0$); (c) waveguide with half lossless ($\varepsilon_c = 1.0$) and half lossy material ($\varepsilon_c = 2.0 - 0.2j$).*

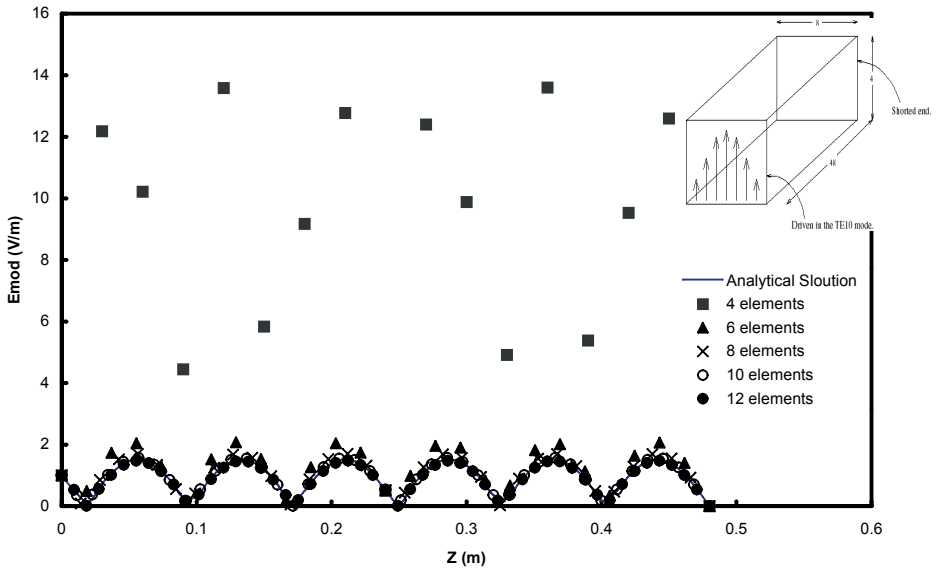

Figure 3: *(a) Distribution of the electric field along the center axis of the shorted waveguide, with lossless media ($\varepsilon_c = 2.0$) for 4 to12 elements per wavelength, and comparison with the analytical solution.* (b) *Comparison of the numerical and analytical solutions for the electric field distribution along the center axis of the shorted waveguide, with a dielectric load in the back half ($\varepsilon_c = 2.0 - 0.2j$) and air ($\varepsilon_c = 1.0$) in the front half. There are 10 elements per wavelength.*

propagated from the magnetron through a WR-975 waveguide and was then fed into the applicator cavity. A microwave power level of 5.0 kW was delivered to the load to obtain a reasonable heating time of 1 minute for a 20 to 80 ºC rise in the food temperature while minimizing the influence of heat conduction.

Because non-uniformity is inherent in microwave heating, we selected the center as a reference location to measure the temperatures. An optic probe sensor was used for this study (FISO Technologies Inc., Sainte-Foy, Quebec, Canada). This fiber optic sensor has 0.1 ºC of resolution, measures a wide temperature range of 40 to 250 °C, and provides a precision of ± 1.0 ºC. Microwave heating was stopped when the central temperature measured by the fiber optic sensor reached 80 ºC. The food sample was removed from the applicator cavity and opened immediately for the temperature measurement.

The surface temperature of the food product was measured with an infrared camera (model Thermal CAM™ SC-300, N. Billerica, MA). The ThermaCAM SC-300 QWIP sensor provided an imaging resolution of 160x120 pixels and captured real-time dynamic events using the camera's digital output at 5 images per second. This camera is capable of analyzing individual frames covering a wide temperature range (-40 to 120 °C) and providing an accuracy of either ±2% of the range or ± 2.0 ºC. The measured temperature range in our studies is 20 to 80 ºC. The emissivity and other measuring parameters such as the measuring distance, ambient temperature, and humidity had been calibrated and set before the tests.

RESULTS AND DISCUSSION

The above computational model enables the prediction of full 3-D electromagnetic and thermal fields, both in transient and steady states, in electromagnetic processing systems for dielectric and electrically conducting materials. For the later, the electrical conductivity is used in place of the imaginary dielectric constant in Eq. (1). Extensive numerical simulations were carried out using the model. The computational results were checked with analytical solutions for simple and idealized systems and compared with the experimentally gathered measurements. The comparison with the analytical solutions was also used to resolve the issues concerning the mesh sensitivity of the numerical simulations. All the testing and numerical simulations were performed on an 8-processor Alpha machine with 8 GB RAM. The integrated model is capable of performing both mutual and one-way coupled analyses. A selection of the results from one-way coupling simulations is presented below.

Numerical Performance

Prior to considering the modeling results, some issues concerning the computational aspects of the 3-D model deserve a discussion. The edge finite element formulation results in a large sparse matrix, which may be solved by either the iterative solvers or direct solvers. The appropriate choice of a solver is crucial for 3-D simulations. Our extensive testing of many available iterative and direct methods indicates that the iterative solvers require approximately one tenth of the memory needed for the direct solver. For example, for a model problem that has more than one million variables, approximately 6.4 GB memory is required if the best renumbering permutations are applied, assuming the double complex precision. This is in contrast with 0.6GB required for iterative solvers. However, selecting appropriate parameters such as preconditioners to obtain converged solutions can be quite intriguing as well as very difficult. For a small to moderately-sized problem, which has unknowns of 300,000 or fewer, direct solvers with appropriate ordering and symbolic factorization seem to perform faster than the iterative solver, even with an appropriately selected pre-conditioner.

While the results presented in this paper are for one-coupling calculations, the model for mutual coupling calculations has also been tested. The details of the mutual coupling and testing can be found in a recent thesis [Akarapu, 2003].

Comparison with Analytical Solution

To test the model predictability, the numerical model is compared with available analytical solutions for various conditions [Balanis, 1989]. These analytical solutions have also been used to guide the design of appropriate meshes for the numerical simulations reported below. Figures 2(a) to 2(c) show the finite element mesh and electric field distributions in two different cases. The waveguide has a cross-section of 8 cm by 4 cm and is 48 cm long. The frequency of excitation for this analytical test case only is 1910 MHz. The waveguide is excited at the bottom in the TE_{10} mode and is shorted at the top end.

Figures 3 (a) and (b) compare the electromagnetic field distribution along the centerline of the rectangular microwave waveguide filled with a lossless medium and half-filled with a lossy medium. For this problem, the analytical solution for the waveguide can be solved using the method of separation of variables [Akarapu; 2003]. Examination of Figure 3 illustrates that excellent agreement is obtained between the analytical and edge finite element results, thus validating the numerical formulation presented above. In figure 3(b), note also that the sharp change in the field distribution near the interface

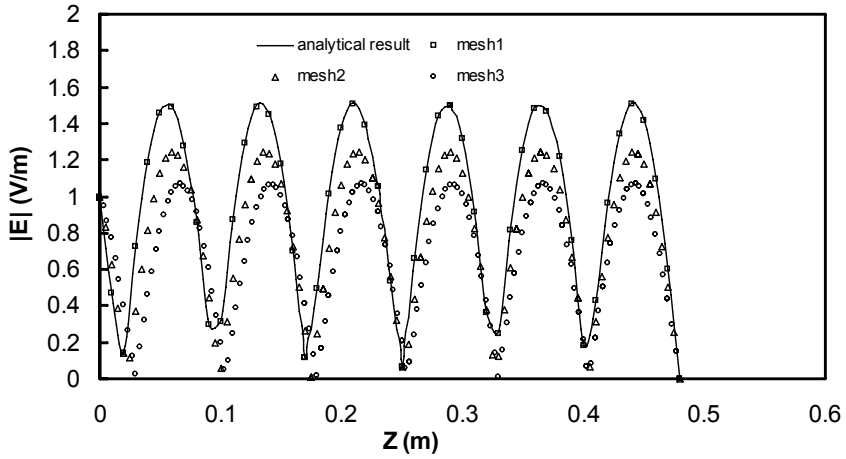

Figure 4. *Effect of element shape regularity on the accuracy of field calculation: (a) mesh 1 with 48 division in the Z direction, 8 divisions in the X direction and 4 divisions in the Y direction; (b) mesh 2 with 96 division in the Z direction, 8 divisions in the X direction and 4 divisions in the Y direction; (c) mesh 3 with 144 division in the Z direction, 8 divisions in the X direction and 4 divisions in the Y direction.*

between the air and lossy medium and the attenuation in the lossy medium is well predicted numerically.

Mesh Sensitivity Testing

The above problem is also used to test the mesh sensitivity, which is found to be very important for microwave simulations. These cases have also been used for mesh sensitivity studies to obtain appropriate criteria for the selection of meshes for numerical simulations. Figure 3(a) shows the results for the lossless case. Inspection of Figure 3(a) suggests that an appropriate resolution of the electromagnetic field in a dielectric material requires about 8 to 10 elements per wavelength. This finding is consistent with the standard FDTD "rule of thumb" suggesting the use of ten cells per wavelength in the medium ($\text{cell size} \le c/10\sqrt{\varepsilon_r}$) and other rules [Dibben and Metaxas; 1997].

The finite element simulations using the tetrahedral edge elements may be very sensitive to their shape regularity. The condition of the field representation deteriorates when tetrahedral edge elements are not well-shaped [Mur; 1994]. The shape quality of the tetrahedral elements is measured quantitatively by [Liu and Joe; 1996]

$$\eta(T) = \frac{12(3V)^{2/3}}{\sum_{0\le i<j\le 3} l_{ij}^2} \qquad (17)$$

where η is the shape quality number, V is the volume, and l_{ij} is the length of the edge. The quality is 1.00 for tetrahedral elements with equal-length edges, and the values drop down for distorted elements. This shape quality indicator indicates how distorted the element is. This mesh shape sensitivity is illustrated by calculating the electric field in the shortened rectangular wave with lossless medium, as shown in Figure 4. This problem is solved using three meshes; almost all elements are of the same shape position in a mesh. The element shape quality number for Mesh1, Mesh2 and Mesh3 are 0.84, 0.706, and 0.485 respectively. The electric field along the centerline of the waveguide is plotted in Figure 4 along with the analytical solution. The results show that the field is deteriorated with elements of bad shape even if the number of elements is increased. Thus, the edge elements with approximately equal edges should be used when possible. The mesh with shape quality < 0.84 should be avoided. For the present work, the results are calculated using meshes with quality factor ≥ 0.84.

Microwave heating of the food package

Let us now consider the microwave thermal processing of food packages. A typical design of a microwave cavity for industrial microwave processing of food packages, as shown in Figure 1, is discretized using 309,120 tetrahedral edge elements. The direct solver with the Multiple Minimum Degree ordering algorithm was used for the solution of the sparse matrix resulting from edge finite element formulation. With 6 microprocessors running in parallel, the calculation required approximately 10 minutes of CPU time on the GS80 platform for the electric field calculations and an insignificant amount of

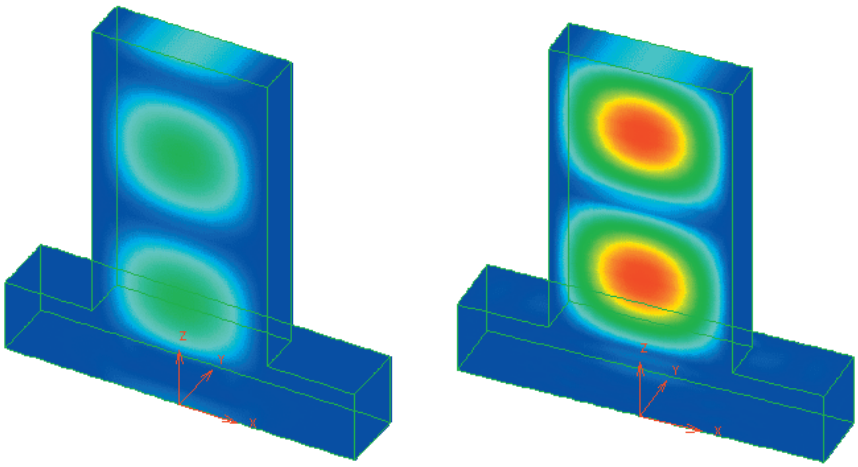

(a) (b)

(a-b) 3-D view of |**E**| distribution

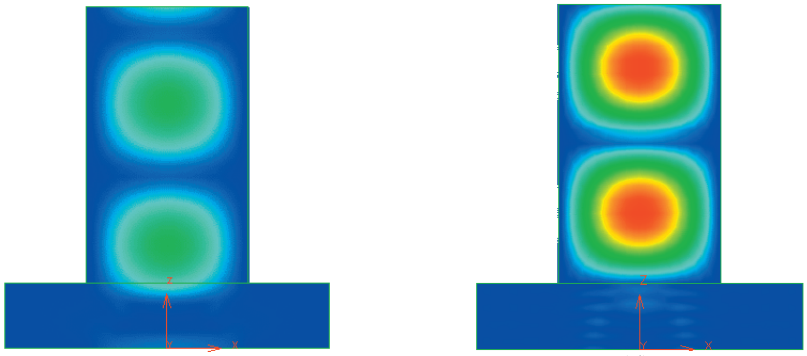

(c) (d)

(c-d) 3-D center cutting view on the x-z surface

Figure 5. *Electric field (|**E**|) distribution in the microwave applicator loaded with a food package (140 X 100 X 30 mm). The top part of the microwave applicator is the standard MR-975 with the height of 52.29 mm and the bottom cavity dimensions (496 X 192 X 100 mm). (a) and (c): the food package is exposed to air and (b) and (d) the food package is immersed in water.*

time for the transient thermal calculations. The materials properties used for the calculations are given Table 1.

The computed electric field distributions in the microwave cavity with TE_{10} model are shown in Figure 5 for two cases. In one case the food package is exposed directly to air. In the other case, the food package is immersed in water, which fills a portion of the bottom cavity from 0 mm to 75 mm in the z-direction. The 3-D view of the contour distribution of the modulus of the electric field on the computed model through the cavity is given in Figures 5(a) and 5(b). Following the guidelines from the mesh sensitivity study, a denser mesh with 10 elements per wavelength is used for the water case. The projection view of the field distribution is shown in Figures 5(c) and 5(d). These figures show the typical features of electromagnetic distribution in both the guide and the cavity portions.

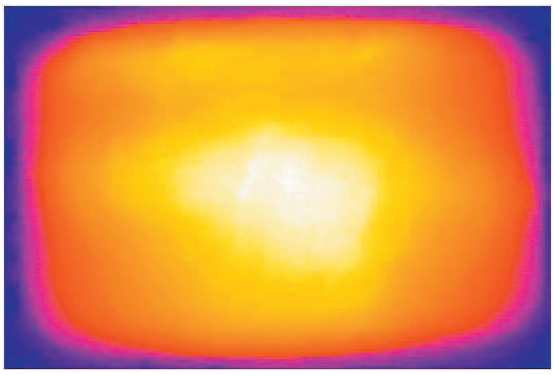

(a) experimental

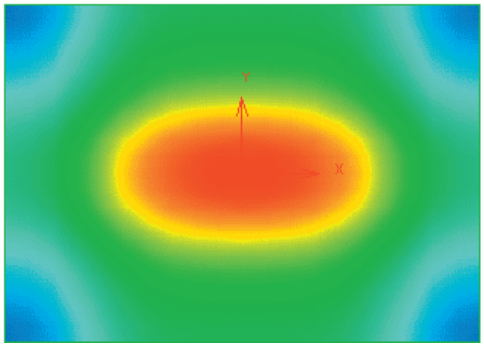

(b) numerical

Figure 6. *Temperature distribution of food packet place in air: (a): Temperature band plot for the entire food packet; (b) Temperature band plot at the center of food packet; (c) Experimental temperature over the top surface of a food gel slab package. Max=77 °C and Min=32 °C. The calculated hot spot on the top surface (a) is at 56 °C.*

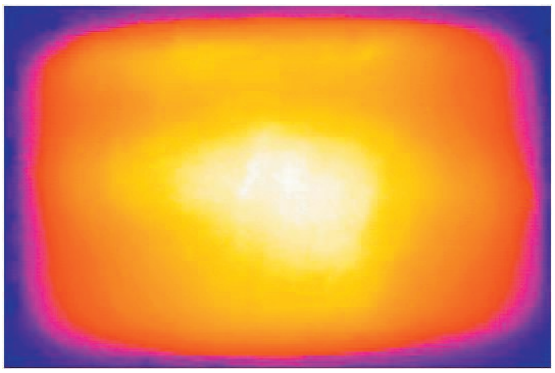

(a) experimental

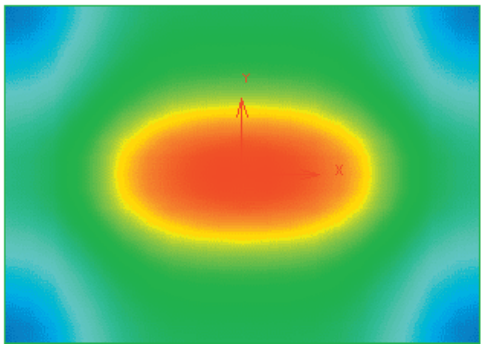

(b) numerical

Figure 7. *Temperature distribution over top surface of a food gel slab package: (a) experimental data are obtained using the infrared camera; (b) numerical data are calculated using the coupled electromagnetic and thermal model (FEM). Parameters for calculations are the same as those in Figure 5 with the water layer (496 X 92 X 75mm).*

The temperature distribution in the food packaged is shown in Figure 6. Figures 6(a) and 6(b) are two different 3-D views of temperature distribution at the top of the surface and at the central plane. As a comparison, Figure 6(c) also plots the experimentally measured temperature distribution, which is measured using an infrared camera. Clearly, the measured heating pattern compares well with that predicted by the integrated microwave-thermal model. In fact, the highest temperature predicted is 10% less than its measured counterpart. In this case, the microwave power is absorbed at the two ends of the food package. The highest temperatures are located near the two edges. The symmetry of the temperature distribution is consistent with the placement of the food package, which is located at the middle of the cavity. From the edge towards the middle, the heating intensity is reduced while there seems to be a relatively strong heating near the center of the food package. The heating pattern is attributed to the fact that the microwaves undergo multiple reflections on the wall and the food load when the wave is launched into the bottom cavity, which is a multi-mode applicator. It is thought that this multi-mode applicator is configured with two major kinds of resonant frequencies. One frequency induces the high hotspots on two sides of the boundary, while the other yields the lower hotspot at the center of the food package.

Figure 7 compares the temperature distribution calculated by the 3-D microwave-thermal model to that measured using the infrared camera for the case in which the food package is immersed in water and both the food package and the water are heated by the microwaves. The comparison between the experimentally measured

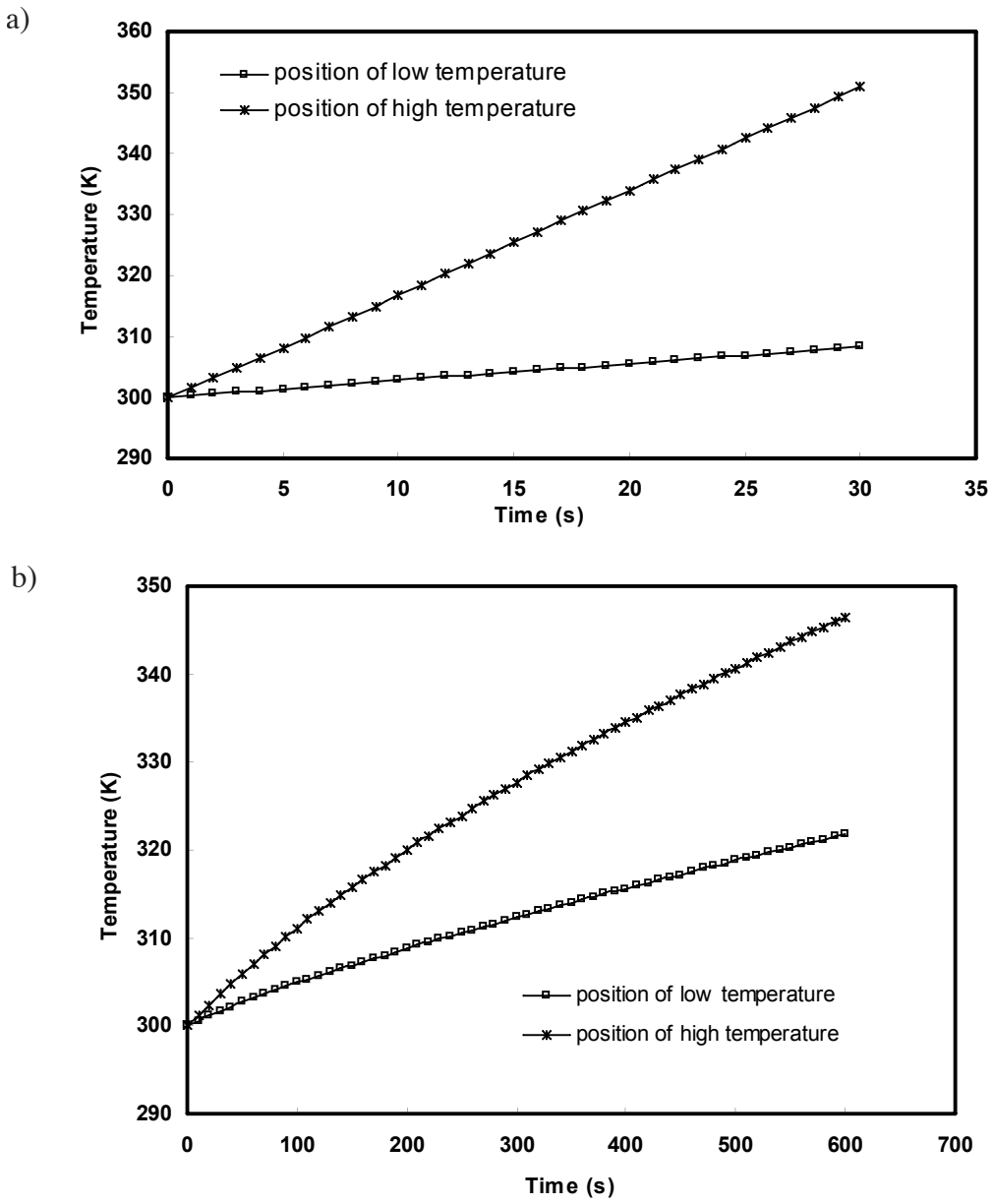

Figure 8. *Evolution of the temperature of the hot and cold spots in the food package heated by microwaves in the applicator with the package immersed in air (a) and in water (b).*

and numerically calculated heating pattern is gratifying. Both show that with the water present, the microwave is absorbed in the central region of the food package, which causes the hot spot to occur in the central region of the package. This is in sharp contrast to the case where the food package is exposed directly to air in the cavity. The results suggest that the surrounding water helps to redistribute the microwave heating power so that the electric power is delivered to the central region of the food package. The heating pattern can be explained by only one major resonant frequency occurring at the central region of the food package.

Figure 8 depicts the temperature histories of the hot and cold spots in the microwave heated package for both cases. As expected, the hot spot heats more rapidly and the cold spot less rapidly, revealing the fact that the absorbed microwave power helps to ramp up the temperature in the package. Also, exposed to air in the applicator, the food package would take 0.5 minutes for the temperature to reach the highest temperature of 77 ^{0}C in the package (see Figure 8a). This compares with the water case where the highest temperature of 73 ^{0}C is reached in ten minutes when a portion of the bottom cavity is filled with water, as shown in Figure 8(b). Inspection of the results further

illustrates that the microwave heating is more effective when the food package is not immersed in water. However, with the presence of water, the difference between the highest and lowest temperatures in the package is smaller about 30 ^{0}C in ten minutes, as shown in Figure 8(b). This phenomenon should be expected because water helps redistribute the microwave energy and make the field distribution relatively more uniform in the food package, in addition to shifting the heating pattern.

As a test, the mutual coupling analysis is also performed for the above two cases using the same properties. The simulation takes considerably longer, and the results, as expected, are the same as those shown in one-way coupling analyses.

CONCLUSION

An integrated electromagnetic and thermal model has been developed for the microwave thermal processing systems. The edge-based finite element method has been employed for solving 3D Maxwell's equations by discritizing the vector wave equation with the electric field as the primary variable. This model is then coupled with the node-based finite element model for thermal calculations. The finite element model has been tested rigorously with simple semi-infinite dielectric problems. The integrated electromagnetic-thermal model can be used to carry out both mutual and one-way coupling analyses. The formulation has compared well with analytical solutions. Mesh sensitivity and shape regularity for the edge element based formulation for computational electromagnetics were also investigated. These guidelines have been used to perform the numerical simulations for microwave food processing in a pilot scale microwave applicator. The calculated results are compared with the experimentally measured data for thermal fields generated by microwave heating in a whey protein gel package, and reasonably good agreement between the two is obtained.

ACKNOWLEDGEMENT

The authors greatly acknowledge the financial support of IMPACT Center (Grant #3). Helpful discussions with Drs. S. Chan and V. Sovar are also acknowledged.

REFERENCE

Akarapu, R. [2003]. Finite Element Modeling of Electromagnetic and Thermo-mechanical Phenomena in Laser and Microwave Processing Systems, (Master thesis, Washington State University)

Balanis, C.A., [1989]. Advanced engineering electromagnetics. Wiley

DeCareau, R.V., [1985]. Microwaves in the Food Processing Industry. Academic Press, Inc., New York.

Demmel, J. W., Eisenstat, S. C., Gilbert, J. R. and Li, X. S. [1999 a]. An asynchronous parallel supernodal algorithm for sparse Gaussian elimination, SIAM J. Matrix Analysis and Applications, 20 (4): 915-952

Demmel, J. W., Eisenstat, S. C., Gilbert, J. R., Li, X. S. and Liu, J. W. [1999 b] A supernodal approach to sparse partial pivoting, SIAM J. Matrix Analysis and Applications, 20 (3): 720-755

Dibben, D. C. and Metaxas, A. C. [1997]. Frequency domain vs. time domain finite element methods for calculation of fields in multimode cavities, IEEE Transactions on Magnetics, 33 (2), 1468-1471

George, A. and Liu, J. W. [1984]. Computer solution of large sparse positive definite systems, Prentice Hall, Englewood, NJ

Haala, J. and Wiesbeck, W. [2000]. Simulation of microwave, convectional and hybrid ovens using a new thermal modeling technique, Journal of Microwave Power and Electromagnetic Energy 35(1): 34-43

Huo, Y. and Li, B. Q. [2004]. three-dimensional marangoni convection in electrostatically positioned droplets under microgravity, Int. J. Heat Mass Trans., 47 pp.3533-3547

Jackson, J. D. [1999]. Classical Electrodynamics- Third Edition, Wiley

Jin, J. [1993]. The Finite Element Method in Electromagnetics, Wiley

Kraus, J., Fleisch, D. [1998]. Electromagntics with Applications, McGraw-Hill

Lu, L., Tang, J. and Liang, L. [1998]. Moisture distribution in spherical foods in microwave drying, Drying Technology 16(3-5): 503-524

Liu, A. and Joe, B. [1996] Quality local refinement of tetrahedral meshes based on 8-subtetrahedraon subdivision, Mathematics of computation, 65: 1183-1200.

Metaxas, A. C. [1996]. Foundations of Electroheat- First Edition, Wiley

Metaxas, A. and Meredith, R. [1983]. Industrial Microwave Heating, Peter Peregrinus, London, U.K

Murr, G. Edge elements, [1994] their advantages and their disadvantages, IEEE transactions on magnetics, 30 (5): 3552-3557

Neophytou, R. and Metaxas, A., [1996]. Computer Simulation of a Radio Frequency Industrial System, Journal of Microwave Power and Electromagnetic Energy, 31(4):251-259.

Pathaka, S. K., Liu, F. and Tang, J. [2003]. Finite difference time domain (FDTD) characterization of single mode applicator. Journal of Microwave Power and Electromagnetic Energy, 38 (1):1-12.

Perkin, R. [1980]. The Heat and Mass Transfer Characteristics of Boiling Point Drying Using Radio Frequency and Microwave Electromagnetic Fields, International Journal of Heat and Mass Transfer, 23: 687-695.

Peyre, F., Datta A,K. and Seyler, C. [1997]. Influence of the dielectric property on microwave oven heating patterns, application to food materials, Journal of Microwave Power and Electromagnetic Energy, 33(4) 243-262.

Piperno, S. and Fezoui, L. [2003]. A centered discontinuous Galerkin finite volume scheme for the 3D heterogeneous Maxwell equations on unstructured meshes, Rapport de recherché 4733, INRIA

Tang, J., Lau, M.H., Taub, I.A., Yang, T.C.S., Kimbell, R., Edwards, C.G., and Younce, F.L. [1999a]. Microwave HTST processing of foods in pouches and trays, AIChE-COFE, Dallas, TX.

Tang, J., Wig, T., Hallberg, L., Dunne, C.P., Koral, T., Pitts, M., Younce, F. [1999b]. Radio frequency sterilisation of military rations AIChE-COFE, Dallas, TX, Paper T3017-66b.

Volakis, J. L., Chatterjee, A. and Kempel, L. C. [1998]. Finite element method for electromagnetics: antennas, microwave circuits, and scattering applications, IEEE press

Watanabe, W. and Ohkawa, S. [1978]. Analysis of Power Density Distribution in Microwave Ovens, Journal of Microwave Power and Electromagnetic Energy, 13(2):173-182.

Zhang, H. and Datta, A. [2000]. Coupled Electromagnetic and Thermal Modeling of Microwave Oven Heating of Foods, Journal of Microwave Power and Electromagnetic Energy**,** 35(2)71-85.

Zhao, H. and Turner, I. [1996]. An Analysis of the Finite-difference Time-Domain Method for Modeling the Microwave Heating of Dielectric Materials Within a Three-Dimensional Cavity System, Journal of Microwave Power and Electromagnetic Energy, 31(4):199-214.

Zeng, X. and Feghri, A. [1994]. Experimental and Numerical Study of Microwave Thawing Heat Transfer for Food Materials, Journal of Heat Transfer, 116:446-455.